RESEARCH ARTICLE

ADVANCED OPTICAL MATERIALS
www.advopticalmat.de

Ultrafast All-Optical Control of Light Chirality with Nanostructured Graphene

Nikolaos Matthaiakakis, Sotiris Droulias, and George Kakarantzas*

Ultrafast nanophotonics is a rapidly growing area of study focused on creating nanodevices that can modulate the properties of light at, to this date, unparalleled speed. To facilitate the growth of this field, there is a growing need for compact metamaterial designs for the manipulation of the amplitude, phase, and polarization of light. One promising strategy involves leveraging the optical nonlinearity of nanostructured materials to alter their permittivity by interacting with high-intensity ultrashort laser pulses. This study showcases how such requirements can be met through the utilization of 2D materials, particularly graphene. The nonlinear optical response of a graphene nanorectangle array is theoretically modeled to achieve all-optical, fully reversible, broadband, and ultrafast dynamic control of light chirality. This is achieved by taking advantage of the energy relaxation dynamics of coherently excited localized plasmons supported by the metasurface, and the transient increase in electron temperature in graphene. Using finite-difference time-domain simulations, ultrafast dynamic tuning between circular and linearly polarized light is demonstrated. The proposed platform gives promise for ultrathin, CMOS-compatible nanophotonic systems that can provide high-speed, room-temperature modulation of light polarization.

1. Introduction

In the past decade, there has been a notable increase in the adoption of specially crafted optical nanomaterials, with a particular emphasis on 2D structures falling within the broader category of nanophotonic structures known as metasurfaces. These metasurfaces represent an innovative avenue for manipulating and guiding light.[1–5] Recent research highlights the utilization of nonlinear nanostructures and metasurfaces, demonstrating their capacity for ultrafast light manipulation when exposed to powerful femtosecond laser pulses.[1,6–9] The temporal dynamics that occur after photoexcitation have been the subject of significant theoretical and experimental investigation, especially in relation to plasmonic nanostructures and metasurfaces. Conductive nanostructures possess localized surface plasmons (LSPs) which upon resonant photoexcitation, rapidly dephase, resulting in the generation of a population of highly energetic electrons in the conductor.[9] Termed "hot" electrons and holes, these carriers exist in a non-equilibrium state, possessing substantially higher energies than their counterparts in thermodynamic equilibrium. They undergo an ultrafast relaxation process (marked by dissipation through environmental equilibration and heat conversion) eventually returning to equilibrium. This process results in a temporal increase in carrier temperature within the conductive nanostructure. This temporal carrier temperature increase can be used to facilitate multiple processes, like driving photochemical reactions on the surface of the metallic nanostructures to enhance catalytic yields,[10–12] aggregating carriers to improve photodetection and photovoltaics,[13–15] and manipulating light with unparalleled speed,[16–18] that are otherwise unattainable. These applications represent just a few of the fascinating possibilities that have been explored thus far.

Graphene exhibits a diverse intrinsic nonlinear optical behavior.[19,20] In the optical and near-infrared spectrum, this behavior is predominantly ascribed to transient Pauli blocking, leading to ultrafast saturable absorption and nonlinear refraction[21] Conversely, in the mid-infrared (mid-IR) and terahertz (THz) range, the nonlinear response is mainly driven by rapid thermal heating and cooling of the electron population, influencing intraband absorption.[22–24] These rapid thermal heating and cooling characteristics of graphene position it as an optimal material for ultrafast nonlinear optical processes within the THz and mid-IR spectral range, especially when compared to other metal conductors typically used in the field of plasmonics.[25,26] Similar to metals, the graphene light-matter

N. Matthaiakakis, G. Kakarantzas
Theoretical and Physical Chemistry Institute
National Hellenic Research Foundation
NHRF
48 Vassileos Constantinou Ave., Athens 11635, Greece
E-mail: nmatth@eie.gr
N. Matthaiakakis
Institute of Nanoscience and Nanotechnology
National Center for Scientific Research "Demokritos"
Ag. Paraskevi 15341, Greece
S. Droulias
Department of Digital Systems
University of Piraeus
Piraeus 18534, Greece

The ORCID identification number(s) for the author(s) of this article can be found under https://doi.org/10.1002/adom.202303181

DOI: 10.1002/adom.202303181

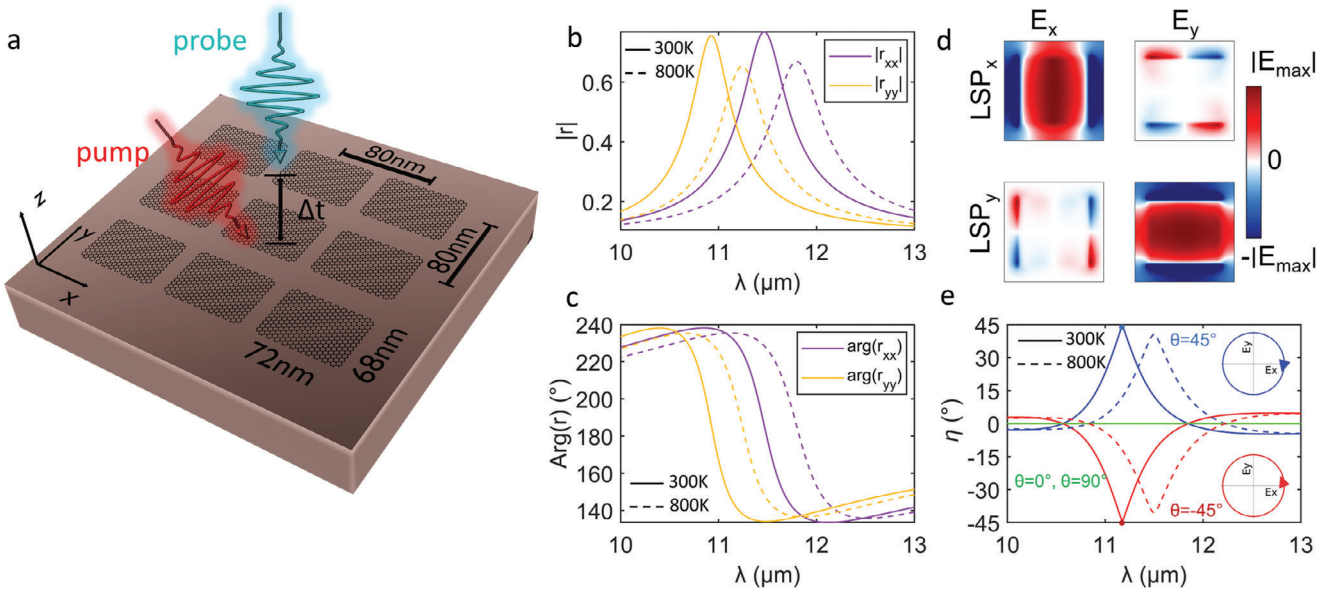

Figure 1. Modal analysis of the graphene metasurface and performance for electron temperatures of 300 and 800K. a) Schematic of the graphene nanorectangle metasurface (width w = 72 nm, height h = 68 nm). The unit cell is periodically repeated in the x- and y-axis with a periodicity p = 80 nm. b) Magnitude and c) phase of the reflection coefficients r_{xx}, r_{yy} (yellow and purple lines respectively) for 300K (solid lines) and 800K (dashed lines). d) x- and y- components of the LSP modes supported by the metasurface units. e) Ellipticity η for source polarization angle $\theta = 45°$(blue), $\theta = 0°$, 90°(green), and θ −45°(red) for electron temperatures of 300K (solid lines) and 800K (dashed lines). Polarization ellipses for the wavelengths of maximum ellipticity (insets).

interactions can be significantly amplified through leveraging plasmon resonances. What sets graphene apart is the added benefit of being able to control these resonant frequencies not just by manipulating the dimensions of graphene structures but also by modifying its carrier concentration through various means, including chemical doping,[27] acoustic excitations[28], and electrical gating.[29–33] Most importantly, by taking advantage of the rapid thermal heating and cooling of graphene, the plasmon resonances can be tuned all-optically and in ultrafast timescales.[24,34] Therefore, graphene proves to be well-suited for a diverse range of all-optical ultrafast functionalities within the THz and mid-IR spectral range.

Recently, there has been significant interest in polarization switching, particularly in the context of ultrafast and all-optical polarization switching,[16,24,35–37] as a functionality with wide-ranging applications in photonics and other fields.[38–41] In this work, to address this exciting challenge, we propose a novel configuration to achieve ultrafast polarization control by employing an experimentally verified thermal model of the nonlinear plasmonic response of graphene.[24] Through Finite-Difference Time-Domain (FDTD) simulations, we showcase the ability to dynamically and all-optically manipulate the polarization states of the reflected light on ultrafast timescales, specifically in the range of a few picoseconds. Achieving this control involves patterning a single-layer graphene sheet into nanorectangles with geometrical anisotropy and initiating a temporal elevation of the free electron temperature using a pump pulse. The time-resolved response of the graphene metasurface can be investigated by employing a probe pulse at various time intervals between the pump and probe pulses. The proposed metasurface's anisotropic nanorectangles support LSPs with different resonance frequencies along the nanostructures' long and short axes, ensuring non-degeneracy. When the resonance frequency of the LSPs aligns with that of the probe pulse, a coherent excitation occurs, shaping the phase profile of the reflected light. As a result of the phase difference of the two orthogonal LSPs, we can attain any desired polarization state, spanning from linear (LPL) to circularly polarized light (CPL). Notably, we demonstrate that ultrafast all-optical dynamic control of polarization conversion can be accomplished by exciting the graphene metasurface with a pump pulse, leading to rapid electron thermalization and de-thermalization. This process shifts the plasmon resonances, facilitating ultrafast polarization switching of the reflected light. Through our findings we aim to provide a methodology for the realization of polarization control in ultrafast photonic systems, using compact and extremely thin nanophotonic devices.

2. Proposed Design and Principle of Operation

The proposed metasurface design is composed of an array of single-layer graphene nanorectangles. The nanorectangles have a width (w) of 72 nm, a height (h) of 68 nm, and a periodicity (p) of 80 nm. They are supported by a substrate with a refractive index n = 1.2, as depicted in **Figure 1a**. The chosen dimensions of the graphene nanorectangles are flexible and can be designed to enable the support of two orthogonal dipole LSP modes within the desired frequency range (in this case 10 −13 μm). By choosing different dimensions and/or Fermi levels the metasurface could operate at any desired wavelength from the mid-IR to the THz range where graphene localized plasmons are supported.[31,42] The contrast between the width and height of the nanorectangles ensures that the degeneracy of the two orthogonal dipole LSPs is lifted,

resulting in different resonant frequencies for each. The extent of the frequency split depends on the contrast between the width and height (aspect ratio), offering flexibility in choosing the exact dimensions of the nanorectangle to tune the plasmon resonances of the metasurface (more details in the Supporting Information).

The optical properties of graphene are modeled using a temperature-dependent Drude model[24] with a Fermi level of 0.35 eV and a mobility value of 27 000 $cm^2\ V^{-1}\ s^{-1}$[43–45] (results for lower mobility values available in the Supporting Information). For the frequencies of interest in this study, graphene operates in the metallic regime, and interband transitions can be neglected. The graphene conductivity is calculated as

$$\sigma(\omega) = \frac{D}{\pi(\Gamma - i\omega)} \tag{1}$$

where Γ is the temperature-dependent scattering rate, and can be calculated as[24]

$$\Gamma(T) \simeq \Gamma_0 \left(1 + \frac{\pi^2 k_B^2 T^2}{6\epsilon_F^2}\right) + \frac{\varepsilon_F V_D^2 k_B T}{4\hbar^3 v_F^2 \rho s^2} \tag{2}$$

and D, the temperature-dependent Drude weight of graphene, as[24]

$$D(T) \simeq \frac{2e^2\varepsilon_F}{\hbar^2}\left(1 - \frac{\pi^2 k_B^2 T^2}{6\epsilon_F^2}\right) \tag{3}$$

where v_F *is* the fermi velocity, ω the radial frequency, e the electron charge, $\hbar$ is the reduced Planck constant, k_B the Boltzmann constant, s is the speed of sound in graphene, ρ is the areal mass density, and V_D the acoustic deformation potential.

To evaluate the optical response of the metasurface, we conducted FDTD simulations using MEEP[46] (more details in the Supporting Information). The metasurface is subjected to external probing at variable carrier temperatures with a LP electromagnetic wave, which is incident at a normal angle. In the simulations, the magnitude (E_0) and azimuth angle (θ) of the source polarization are defined with respect to the x-axis, as illustrated in Figure 1a which is analyzed in the x- and y- directions as $E_{x,inc} = E_0\cos\theta$ and $E_{y,inc} = E_0\sin\theta$. The temperature-dependent far-field response of the system under probe pulse illumination can be characterized using the scattering matrix. This matrix establishes the relationship between the complex amplitudes of the incident and reflected fields and provides valuable information about how the metasurface scatters and modifies the incident electromagnetic wave.[47,48] The scattering matrix is written as

$$\begin{pmatrix} E_{x,ref} \\ E_{y,ref} \end{pmatrix} = \begin{pmatrix} r_{xx}(T) & r_{xy}(T) \\ r_{yx}(T) & r_{yy}(T) \end{pmatrix} \begin{pmatrix} E_{x,inc} \\ E_{y,inc} \end{pmatrix} \tag{4}$$

where, r_{xx}, r_{yy}, r_{xy}, r_{yx} are the temperature-dependent reflection amplitudes, E_{ref} corresponds to the reflected and E_{inc} to the incident electric field, and the x,y subscripts denote the field components along the x- and y- directions respectively. Here we calculate $r_{xy} = 0$, $r_{yx} = 0$, and $r_{xx} \neq 0$, $r_{yy} \neq 0$, thus the contributions from the x- and y-polarized components to the reflected spectra under any given orientation of the incident light can be described through the reflection amplitudes r_{xx} and r_{yy} as

$$\mathbf{E}_{ref} = r_{xx}(T)E_{x,inc}\mathbf{x} + r_{yy}(T)E_{y,inc}\mathbf{y} \tag{5}$$

Figure 1(b) shows the absolute value and Figure 1(c) the phase of the reflection amplitudes r_{xx} (purple) and r_{yy} (yellow) for two different carrier temperatures $T = 300$K and $T = 800$K (solid and dashed lines respectively). Here we directly introduce this electron thermalization through T in Equations 1–3. In practice such electron thermalization can be achieved by introducing a pump pulse in resonance with the plasmon excitations supported by the metasurface. The electron temperature T in graphene under pump pulse excitation with intensity I(t) and a central frequency ω_0 evolves as

$$\alpha T\frac{dT}{dt} + \beta(T^3 - T_L^3) = A(\omega_0; T)I(t) \tag{6}$$

where αT is the specific heat of graphene with $\alpha = 2\pi {k_B}^2\epsilon_F/(3\hbar^2 {v_F}^2)$, $\beta = \zeta(3){V_D}^2\epsilon_F {k_B}^3/(\pi^2\rho\hbar^4 {v_F}^3 s^2 l)$ is the cooling coefficient, $A(\omega)$ is the fractional absorption in the graphene, ζ is the Riemann zeta function, l is the electron-disorder mean free path, and T_L is the lattice temperature.[24] For the narrow-band terahertz – mid IR pulses analyzed in this study, we can estimate the relationship between the peak temperature (T) and fluence (F) by assuming that the peak temperature and peak intensity occur nearly simultaneously in time, that the pump pulse frequency coincides with the frequency of the maximum absorption max($A(\omega)$), and neglecting the lattice temperature and higher-order temperature-dependent changes in the absorption coefficient A as[24]

$$\beta T_{\max}^3 = A(\omega)I_{\max} \tag{7}$$

where $T_{\max}$ is the peak electron temperature and $I_{\max} = 0.94F/\Delta t_{FWHM}$ the peak intensity of a Gaussian pulse with fluence F and duration Δt_{FWHM}. Thus, for example, a pump pulse with a fluence $F = 2.3\mu J\ cm^{-2}$ and $\Delta t_{FWHM} = 5.5$ ps corresponds to the elevated temperature of 800K assumed in Figure 1b. These values of the pump pulse are similar to those found in experimental works[24] and are well below the damage threshold of graphene.[49–51] The elevated electron temperature causes a redshift of the reflection amplitude peaks and their corresponding phases. This is attributed to the heightened scattering rates and the shift of the Fermi level in graphene caused by carrier thermalization, leading to plasmon resonances that are both redshifted and broadened.[24] For both temperatures, $T = 300$K and $T = 800$K, the spectra of the emitted light corresponding to the x-polarized dipole mode (LSP_x) exhibit peaks at longer wavelengths compared to the y-polarized dipole mode (LSP_y). This disparity is a result of the non-degeneracy of the plasmon modes in the x-y directions, stemming from the anisotropy of the graphene nanorectangles. Furthermore, the phase difference $\Delta\varphi = \arg(r_{yy}) - \arg(r_{xx})$ between the LSP_x and LSP_y exhibits a broad range of values across the entire spectral range of interest, reaching 90°, which is essential for the formation of pure circularly polarized light, as depicted in Figure 1c. Figure 1d illustrates the eigenmodes of the system, the localized surface plasmons (LSP_x and LSP_y). Each LSP mode is characterized by a

radiative dipole component and a nonradiative quadrupole component aligned with the x- and y-directions. The radiative or nonradiative nature of each LSP component arises from the presence or absence of a nonzero net electric or magnetic moment, respectively, along the corresponding polarization direction. It is noteworthy that the radiative dipoles are mutually perpendicular to each other, a crucial aspect defining the operational principle of our configuration.

Equation 4 provides a general description of the metasurface behavior for any source polarization. By analyzing this equation, we can determine the conditions for achieving circularly polarized light in the reflected light. Specifically, the conditions that need to be satisfied are $r_{yy}(T)E_{y,inc} = r_{xx}(T)E_{x,inc}$and $\Delta\varphi = \arg(r_{yy}(T)) - \arg(r_{xx}(T)) = 90°$, where the only adjustable parameters are the source phase and amplitude, and the temperature T. Assuming a constant temperature $T = 300$K, we can manipulate the system's response through a simple rotation of the source polarization angle θ relative to the metasurface. Our findings show that for left-handed (LH) CPL, the desired polarization is achieved at $\theta = 45°$, whereas for right-handed (RH) CPL, it is achieved at $\theta = -45°$, as seen in Figure 1e. For $T = 800$K the peak value of the ellipticity is reduced and is also red-shifted, following the shift of the plasmon resonances.

Edge roughness and fabrication imperfections can result in defects in experimental metasurfaces that can affect the device performance, nevertheless the proposed metasurface operates sufficiently well even for imperfect geometries. Adjustment of the probe pulse polarization according to Equation 5 can also be used to better optimize the metasurface performance in combination with Fermi level tuning. Furthermore, since the metasurface operation is scalable and depends on the aspect ratio rather than the exact size of the nanorectangles, larger metasurface units can be used since they are less sensitive to small experimental imperfections.

3. Temperature Dependence of Reflected Light Polarization

It is useful to further investigate how the response of the system is altered as the electron temperature increases. **Figure 2** shows the FDTD calculated response of the metasurface for a range of temperatures from 300 to 1200K under LP source excitation with $\theta = 45°$. Figure 2a shows the reflectance from the metasurface versus the electron temperature in graphene. Figure 2c,d shows the ellipticity η and rotation α of the reflected light for the same temperature range as in Figure 2a. As the temperature increases there is an increasingly stronger redshift, broadening, and weakening of the plasmon modes supported by the metasurface. Consequently, there is a corresponding shift of the peak ellipticity η and rotation α towards longer wavelengths. This is due to the increased electron scattering and the reduced value of the chemical potential of graphene at elevated electron temperatures[24] Thus, while at $\lambda = 11.15$ μm for $T = 300$K the reflected light is LCP, for elevated electron temperatures it becomes elliptical and even LP.

4. All-Optical Ultrafast Polarization Control

Since the electron temperature in graphene can strongly influence the reflected light polarization from the metasurface, it is interesting to investigate how this can be performed at ultrafast timescales. This is achieved by using Equation 6 to perform pump-probe FDTD simulations. However, performing such calculations demands updating material properties at each timestep of the FDTD simulation to incorporate the pump pulse's effect on the graphene electron temperature and subsequent changes in conductivity. Computationally, such a simulation setup can be very intensive and necessitates multiple repetitions to obtain results for different pump-probe time delays Δt. Instead, as previously demonstrated in good agreement with experimental results[24] we can perform a pump-probe analysis by splitting the problem in a series of linear simulations each corresponding to a specific value of Δt but this time with a static conductivity and only using a probe pulse. In this method, the contribution of the pump pulse for each value of Δt is included through the adjustment of the graphene conductivity in every individual FDTD simulation to account for the change in carrier temperature according to Equation 6. Equation 6 is solved with the use of the Euler method, and Equations 1,2, and 3, for the Drude weight, scattering losses, and conductivity, are updated at each time step of

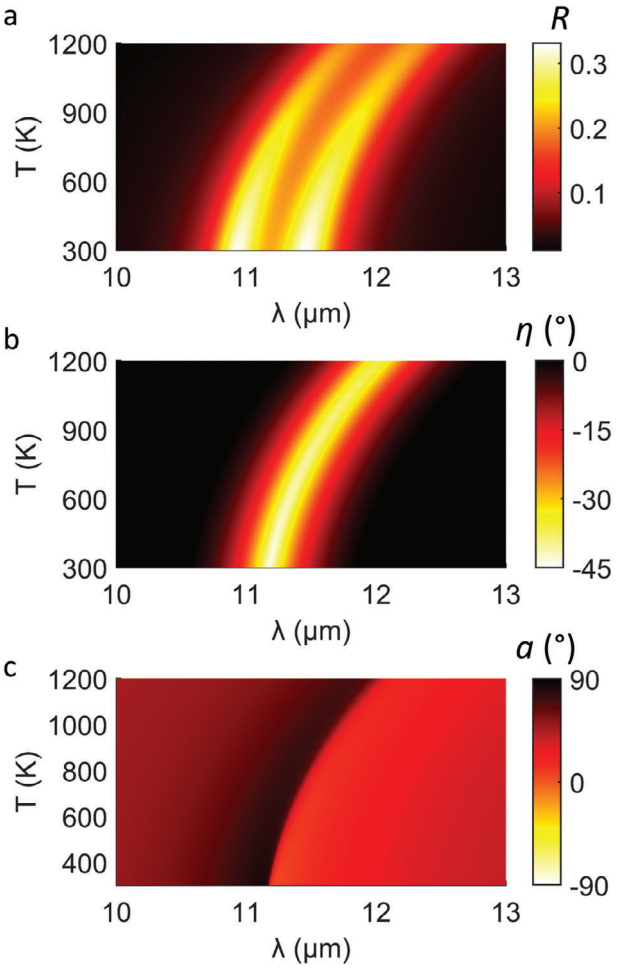

Figure 2. Reflection of the metasurface and polarization states of the reflected light for varying electron temperatures between 300 and 1200K. a) Reflection versus electron temperature. b) Ellipticity η and c) rotation α versus electron temperature.

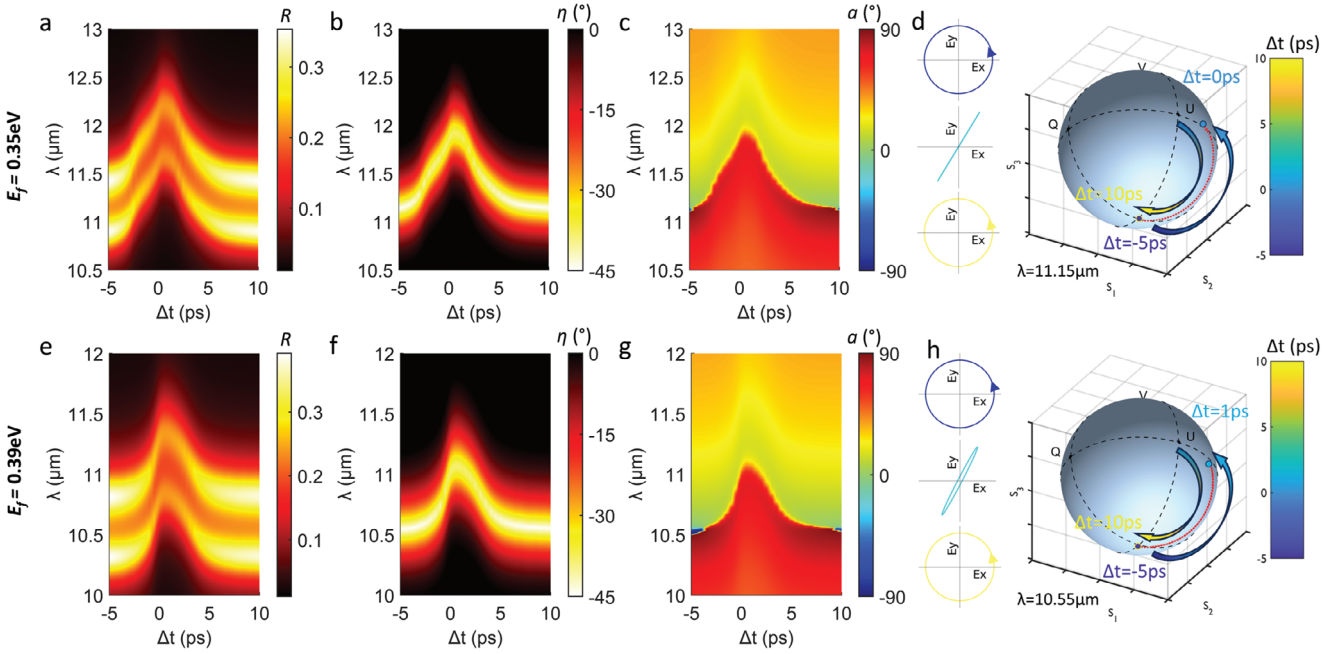

Figure 3. All-optical ultrafast tunning of the metasurface optical properties in a pump probe setup with a pump pulse of intensity $F = 4.44\mu J\ cm^{-2}$ and 3.3 ps FWHM. a) Reflection b) ellipticity η, and c) rotation α modulation for different Δt values between the pump and the probe pulses and $E_f = 0.35$ eV. d) Poincaré sphere showing polarization states for different Δt values between the pump and the probe pulses corresponding to $\lambda = 11.15$ μm of b. e) Reflection f) ellipticity η, and g) rotation α modulation for different Δt values between the pump and the probe pulses and $E_f = 0.39$ eV. h) Poincaré sphere showing polarization states for different Δt values between the pump and the probe pulses corresponding to $\lambda = 10.55$ μm of b.

the solution of Equation 6 according to the calculated electron thermalization. The absorption $A(\omega_0, T)$ for different values of graphene electron temperature T is obtained through FDTD simulations and is adjusted accordingly at each individual time step of the solution of Equation 6 ($A(\omega_0, T)$ and is updated for a step of 50K of temperature difference).

Narrowband pulses have longer durations which interact with a larger part of the transient response of the observed system, thus containing multiple polarization components in time. Broadband pulses on the other hand, have short durations and the interaction of the pulse with the graphene metasurface can be much shorter than a noticeable difference in the transient response of the system. In this case the reflected pulse will contain multiple polarization components at different wavelengths, thus providing clearly defined polarization states at the desired wavelength. To achieve this experimentally ultra-short pulses, like fs pulses[52] can be used, ensuring that the interaction with the graphene metasurface is much shorter than noticeable changes in the transient response of the system (which for the presented metasurface is in the ps timescale). This way high-resolution observations can be performed, accurately capturing the system's response.

Figure 3 shows the ultrafast response of the graphene metasurface for a pump pulse of 3.3 ps and $F = 4.44\mu J\ cm^{-2}$, $\theta = 45°$, and a free space wavelength $\lambda_0 = 11.64$ μm. The pump pulse introduces a temporal carrier thermalization that results in a shift of the plasmon modes supported by the metasurface. As seen in Figure 3a, the peak of the electron thermalization appears to take place at approximately $\Delta t = 0$ ps, resulting in the maximum shift of the plasmon resonances, with a significant falloff between 2–5 ps and the complete electron relaxation process taking place approximately within 10 ps, in good agreement with previous theoretical and experimental works.[24,53,54] The temporal shift of the plasmon modes also results in a shift of the ellipticity η (Figure 3b) and of the rotation α (Figure 3c), allowing ultrafast tuning between CP, elliptically polarized, and LP light within a few ps. Furthermore, a polarization rotation is observed within the same timescale.

Figure 3d shows the Poincaré sphere, as mapped by the Stokes parameters (S_1, S_2, S_3) for the ellipticity and rotation data corresponding to a wavelength of $\lambda = 11.15$ μm in Figure 3b,c, for the entire range of Δt values. The polarization of the emitted light is tuned from CP at −5 ps to LP at 0 ps and back to CP at 10 ps. For the same Δt range there is a notable optical rotation between −5 and 0 ps and between 0 and 10 ps.

With electrostatic tuning, the operation of the metasurface can be extended to a broad range of wavelengths. We demonstrate this additional degree of freedom on the dynamic control of the optical properties of the metasurface by reproducing the results of Figure 3a–d for $E_f = 0.39$ eV in Figure 3e–h. The increase of the graphene Fermi level results in a blueshift of the LSPs and with the pump wavelength now set at $\lambda_0 = 11.23$ μm the metasurface provides efficient and ultrafast polarization conversion at $\lambda = 10.55$ μm. Therefore, depending on the application, the metasurface can be designed to operate across a broad spectral range which can further be tuned by electrostatic control of the graphene Fermi level, offering a versatile platform for ultrafast dynamic manipulation of light polarization over a considerable spectral range from THz to almost near infrared frequencies[42]

5. Discussion and Conclusion

The expanding field of mid and long-infrared photonics is significantly impacting science and technology, with applications spanning diverse domains. Fast modulation of long infrared wavelengths is essential for FTIR spectroscopy, chemical analysis, and environmental monitoring. It also enables high-speed data transmission in free-space optical communication, with potential applications in secure communication through chiral modulation. In security and surveillance, fast-modulated long-wave infrared imaging is crucial, while in biomedical imaging, it aids disease detection through chiral modulation. Additionally, fast modulation in the long infrared range improves accuracy in remote sensing, vital for environmental monitoring and geological surveys. The proposed metasurface could potentially contribute to the development of new technologies in these fields, offering ultrafast tunability, broadband operation, and precise control over both the intensity and polarization of emitted light. As proof of concept, the study of isolated graphene rectangles, either through far-field or near-field probes, could be explored instead of the full metasurface, providing valuable insights into the behavior and properties of individual graphene structures. Nonetheless, the implementation of experimental devices, particularly for potential commercial applications, may encounter challenges. Obtaining high-mobility graphene at the necessary scale for commercial products poses a possible difficulty, potentially affecting performance, as observed in lower mobility metasurfaces studied in this research. Additionally, achieving small and defect-free metasurface dimensions may be challenging. However, since the device's operation relies on the aspect ratio of nanorectangles rather than precise dimensions, larger structures could be employed in experimental setups. Careful design of the experimental pump-probe system is also necessary. The use of ultra-short probe pulses, such as femtosecond pulses, ensures that the interaction with the graphene metasurface is briefer than noticeable changes in the transient response. Addressing potential inhomogeneities in the pump beam optical profile can also prevent uneven heating of the metasurface, which could lead to an averaging of the transient response.

In conclusion, through FDTD simulations, we have explored an atomically thin metasurface that offers a versatile platform for all-optical ultrafast, fully reversible, broadband, and dynamic control over light chirality. By leveraging the energy relaxation dynamics of the coherently excited localized plasmons and the transient increase in electron temperature facilitated by the metasurface and the pump pulse, we have achieved complete and ultrafast polarization control over the reflected light, all the way from linear to circularly polarized light with as low as few ps intervals. The metasurface operates by selectively exciting the localized surface plasmon modes supported by graphene nanorectangles, whose degeneracy is broken due to the anisotropic geometry of the metasurface units. Through the transient heating of the electron population induced by the pump pulse, we can control the ellipticity (η) and rotation (α) of the reflected field, allowing for a wide range of polarization states. While we demonstrate the metasurface's operation at specific Fermi levels, the same principles can be applied for any realistic value for the Fermi level of graphene, allowing operation across a broad spectral range.

Supporting Information

Supporting Information is available from the Wiley Online Library or from the author.

Acknowledgements

The publication of the article in OA mode was financially supported by HEAL-Link.

Conflict of Interest

The authors declare no conflict of interest.

Author Contributions

The manuscript was written through contributions of all authors. NM conceived the idea of this work and performed the simulations and theoretical calculations. SD and GK provided supervision of the project. All authors have given approval to the final version of the manuscript.

Data Availability Statement

The data that support the findings of this study are available from the corresponding author upon reasonable request.

Keywords

all-optical, circularly polarized light, graphene metasurface, localized surface plasmon, ultrafast

Received: December 14, 2023
Revised: February 16, 2024
Published online: March 5, 2024

[1] D. Neshev, I. Aharonovich, *Light Sci. Appl.* **2018**, *7*, 58.
[2] A. V. Kildishev, A. Boltasseva, V. M. Shalaev, *Science* **2013**, *339*, 12320091.
[3] N. Yu, F. Capasso, *Nat. Mater.* **2014**, *13*, 139.
[4] A. I. Kuznetsov, A. E. Miroshnichenko, M. L. Brongersma, Y. S. Kivshar, B. Luk'yanchuk, *Science* **2016**, *354*, aag2472.
[5] T. Phan, D. Sell, E. W. Wang, S. Doshay, K. Edee, J. Yang, J. A. H.-E. Fan, *Light Sci. Appl.* **2019**, *8*, 48.
[6] P. Vasa, C. Ropers, R. Pomraenke, C. Lienau, *Laser Photonics Rev.* **2009**, *3*, 483.
[7] S. V. Makarov, A. S. Zalogina, M. Tajik, D. A. Zuev, M. V. Rybin, A. A. Kuchmizhak, S. Juodkazis, Y. Kivshar, S. V. Makarov, A. S. Zalogina, M. Tajik, D. A. Zuev, M. V. Rybin, Y. Kivshar, A. A. Kuchmizhak, S. Juodkazis, *Laser Photon. Rev.* **2017**, *11*, 1700108.
[8] M. Ren, W. Cai, J. Xu, *Adv. Mater.* **2020**, *32*, 1806317.
[9] A. Schirato, M. Maiuri, G. Cerullo, G. Della Valle, *Nanophotonics* **2023**, *12*, 1.
[10] A. Naldoni, U. Guler, Z. Wang, M. Marelli, F. Malara, X. Meng, L. V. Besteiro, A. O. Govorov, A. V. Kildishev, A. Boltasseva, V. M. Shalaev, A. Naldoni, U. Guler, Z. Wang, X. Meng, A. V. Kildishev, A. Boltasseva, V. M. Shalaev, M. Marelli, F. Malara, L. V. Besteiro, A. O. Govorov, *Adv. Opt. Mater.* **2017**, *5*, 1601031.

[11] S. Mubeen, J. Lee, N. Singh, S. Krämer, G. D. Stucky, M. Moskovits, *Nat. Nanotechnol.* **2013**, *84*, 247.
[12] P. Christopher, H. Xin, S. Linic, *Nat. Chem.* **2011**, *3*, 467.
[13] H. Chalabi, D. Schoen, M. L. Brongersma, *Nano Lett.* **2014**, *14*, 1374.
[14] A. Giugni, B. Torre, A. Toma, M. Francardi, M. Malerba, A. Alabastri, R. Proietti Zaccaria, M. I. Stockman, E. Di Fabrizio, *Nat. Nanotechnol.* **2013**, *8*, 845.
[15] F. Wang, N. A. Melosh, *Nano Lett.* **2011**, *11*, 5426.
[16] L. H. Nicholls, F. J. Rodríguez-Fortuño, M. E. Nasir, R. M. Córdova-Castro, N. Olivier, G. A. Wurtz, A. V. Zayats, *Nat. Photonics* **2017**, *11*, 628.
[17] G. A. Wurtz, R. Pollard, W. Hendren, G. P. Wiederrecht, D. J. Gosztola, V. A. Podolskiy, A. V. Zayats, *Nat. Nanotechnol.* **2011**, *6*, 107.
[18] M. Taghinejad, H. Taghinejad, Z. Xu, K. T. Lee, S. P. Rodrigues, J. Yan, A. Adibi, T. Lian, W. Cai, *Nano Lett.* **2018**, *18*, 5544.
[19] I. A. Calafell, L. A. Rozema, D. A. Iranzo, A. Trenti, P. K. Jenke, J. D. Cox, A. Kumar, H. Bieliaiev, S. Nanot, C. Peng, D. K. Efetov, J.-Y. Hong, J. Kong, D. R. Englund, F. J. García de Abajo, F. H. L. Koppens, P. Walther, *Nat. Nanotechnol* **2021**, *16*, 318.
[20] M. Massicotte, G. Soavi, A. Principi, K. J. Tielrooij, *Nanoscale* **2021**, *13*, 8376.
[21] H. Zhang, S. Virally, Q. Bao, L. Kian Ping, S. Massar, N. Godbout, P. Kockaert, *Opt. Lett.* **2012**, *37*, 1856.
[22] G. Jnawali, Y. Rao, H. Yan, T. F. Heinz, *Nano Lett.* **2013**, *13*, 524.
[23] S. F. Shi, T. T. Tang, B. Zeng, L. Ju, Q. Zhou, A. Zettl, F. Wang, *Nano Lett.* **2014**, *14*, 1578.
[24] M. M. Jadidi, J. C. König-Otto, S. Winnerl, A. B. Sushkov, H. D. Drew, T. E. Murphy, M. Mittendorff, *Nano Lett.* **2016**, *16*, 2734.
[25] F. Kadi, T. Winzer, E. Malic, A. Knorr, F. Göttfert, M. Mittendorff, S. Winnerl, M. Helm, *Phys. Rev. Lett.* **2014**, *113*, 035502.
[26] Z. Mics, K. J. Tielrooij, K. Parvez, S. A. Jensen, I. Ivanov, X. Feng, K. Müllen, M. Bonn, D. Turchinovich, *Nat. Commun.* **2015**, *6*, 7655.
[27] H. Liu, Y. Liu, D. Zhu, *J. Mater. Chem.* **2011**, *21*, 3335.
[28] W. Wang, B. H. Li, E. Stassen, N. Asger Mortensen, J. Christensen, *Nanoscale* **2016**, *8*, 3809.
[29] Z. Fang, S. Thongrattanasiri, A. Schlather, Z. Liu, L. Ma, Y. Wang, P. Ajayan, P. Nordlander, N. Halas, F. de Abajo, *ACS Nano* **2013**, *7*, 2388.
[30] J. Kim, H. Son, D. J. Cho, B. Geng, W. Regan, S. Shi, K. Kim, A. Zettl, Y.-R. Shen, F. Wang, *Nano Lett.* **2012**, *12*, 5598.
[31] L. Ju, B. Geng, J. Horng, C. Girit, M. Martin, Z. Hao, H. A. Bechtel, X. Liang, A. Zettl, Y. R. Shen, F. Wang, *Nat. Nanotechnol.* **2011**, *6*, 630.
[32] Y. Yao, M. Kats, P. Genevet, N. Yu, Y. Song, J. Kong, F. Capasso, *Nano Lett.* **2013**, *13*, 1257.
[33] Y. Li, H. Li, S. Wu, W. T. Liu, *J. Chem. Phys.* **2020**, *153*, 080903.
[34] L. Ju, J. Velasco, E. Huang, S. Kahn, C. Nosiglia, H. Z. Tsai, W. Yang, T. Taniguchi, K. Watanabe, Y. Zhang, G. Zhang, M. Crommie, A. Zettl, F. Wang, *Nat. Nanotechnol.* **2014**, *9*, 348.
[35] Y. Yang, K. Kelley, E. Sachet, S. Campione, T. S. Luk, J. P. Maria, M. B. Sinclair, I. Brener, *Nat. Photonics* **2017**, *11*, 390.
[36] S. Klimmer, O. Ghaebi, Z. Gan, A. George, A. Turchanin, G. Cerullo, G. Soavi, *Nat. Photonics* **2021**, *15*, 837.
[37] A. Schirato, M. Maiuri, A. Toma, S. Fugattini, R. Proietti Zaccaria, P. Laporta, P. Nordlander, G. Cerullo, A. Alabastri, G. Della Valle, *Nat. Photonics* **2020**, *14*, 723.
[38] N. Matthaiakakis, T. Sannomiya, *ACS Appl. Nano Mater.* **2020**, *3*, 6816.
[39] N. Matthaiakakis, S. Droulias, G. Kakarantzas, **2022**, *10*, 2102273.
[40] N. Matthaiakakis, S. Droulias, G. Kakarantzas, *ACS Appl. Opt. Mater.* **2023**, *1*, 952.
[41] S. Biswas, W. Whitney, M. Grajower, K. Watanabe, T. Taniguchi, H. Bechtel, G. Rossmas, H. Atwater, *Sci. Adv. 7*, https://www.science.org/doi/10.1126/sciadv.abd4623.
[42] T. Low, P. Avouris, *ACS Nano* **2014**, *8*, 1086.
[43] A. Tyagi, V. Mišeikis, L. Martini, S. Forti, N. Mishra, Z. M. Gebeyehu, M. A. Giambra, J. Zribi, M. Frégnaux, D. Aureau, M. Romagnoli, F. Beltram, C. Coletti, *Nanoscale* **2022**, *14*, 2167.
[44] L. Banszerus, M. Schmitz, S. Engels, J. Dauber, M. Oellers, F. Haupt, K. Watanabe, T. Taniguchi, B. Beschoten, C. Stampfer, *Sci. Adv.* **2015**, *1*, 1.
[45] D. De Fazio, D. G. Purdie, A. K. Ott, P. Braeuninger-Weimer, T. Khodkov, S. Goossens, T. Taniguchi, K. Watanabe, P. Livreri, F. H. L. Koppens, S. Hofmann, I. Goykhman, A. C. Ferrari, A. Lombardo, *ACS Nano* **2019**, *13*, 8926.
[46] A. F. Oskooi, D. Roundy, M. Ibanescu, P. Bermel, J. D. Joannopoulos, S. G. Johnson, *Comput. Phys. Commun.* **2010**, *181*, 687.
[47] R. C. Jones, *J. Opt. Soc. Am.* **1941**, *31*, 488.
[48] C. Menzel, C. Rockstuhl, F. Lederer, *Phys. Rev. A* **2010**, *82*, 053811.
[49] B. Krauss, T. Lohmann, D. H. Chae, M. Haluska, K. Von Klitzing, J. H. Smet, *Phys. Rev. B* **2009**, *79*, 165428.
[50] M. Currie, J. D. Caldwell, F. J. Bezares, J. Robinson, T. Anderson, H. Chun, M. Tadjer, *Appl. Phys. Lett.* **2011**, *99*, 211909.
[51] A. Roberts, D. Cormode, C. Reynolds, T. Newhouse-Illige, B. J. Leroy, A. S. Sandhu, *Appl. Phys. Lett.* **2011**, *99*, 051912.
[52] K. Tian, L. He, X. Yang, H. Liang, *Photonics* **2021**, *8*, 290.
[53] S. Winnerl, M. Orlita, P. Plochocka, P. Kossacki, M. Potemski, T. Winzer, E. Malic, A. Knorr, M. Sprinkle, C. Berger, W. A. De Heer, H. Schneider, M. Helm, *Phys. Rev. Lett.* **2011**, *107*, 237401.
[54] E. A. A. Pogna, X. Jia, A. Principi, A. Block, L. Banszerus, J. Zhang, X. Liu, T. Sohier, S. Forti, K. Soundarapandian, B. Terrés, J. D. Mehew, C. Trovatello, C. Coletti, F. H. L. Koppens, M. Bonn, H. I. Wang, N. van Hulst, M. J. Verstraete, H. Peng, Z. Liu, C. Stampfer, G. Cerullo, K.-J. Tielrooij, *ACS Nano* **2021**, *15*, 11285.